Multifrequency EPR Study of Metallofullerenes: Eu@C_{82} and Eu@C_{74}

Hideto Matsuoka,[†] Norio Ozawa,[‡] Takeshi Kodama,[‡] Hiroyuki Nishikawa,[‡] Isao Ikemoto,[‡] Koichi Kikuchi,[‡] Ko Furukawa,[†] Kazunobu Sato,[§] Daisuke Shiomi,[§] Takeji Takui,[§] and Tatsuhisa Kato*[,†,⊥]

Institute for Molecular Science, Myodaiji, Okazaki 444-8585, Japan, Department of Chemistry, Tokyo Metropolitan University, Hachioji, Tokyo 192-0397, Japan, Departments of Chemistry and Materials Science, Graduate School of Science, Osaka City University, Sugimoto 3-3-138, Sumiyoshi-Ku, Osaka 558-8585, Japan, and Department of Chemistry, Josai University, Keyakidai 1-1, Sakado, Saitama 350-0295, Japan

Received: December 31, 2003; In Final Form: June 21, 2004

In this work, the cage structure of a family of europium metallofullerenes, Eu@C_{74} and three isomers of Eu@C_{82}, were investigated. The analogy of the electronic states of three isomers of Eu@C_{82} with those of three isomers of Ca@C_{82} was confirmed by UV−vis−near-IR absorption spectra. The symmetries C_s, C_2, and C_{2v} were assigned for three isomers of Eu@C_{82} by comparing each corresponding isomer of Ca@C_{82}. The D_{3h} cage structure of Eu@C_{74}, which is expected only for the C_{74} from the isolated pentagon rule, was also confirmed by comparing its photoabsorption spectrum with that of Ca@C_{74}. Multifrequency electron paramagnetic resonance (EPR) spectroscopy was employed to determine the zero-field splitting (ZFS) parameters of the metallofullerenes, which are closely related to the surrounding cage structures. The experimental X- and W-band EPR spectra were completely reproduced by computer simulations based on a spin Hamiltonian considering the ZFS terms up to fourth order. The introduction of the fourth-order ZFS terms into the Hamiltonian resulted in a precise determination of the second-order ZFS terms. A nonvanishing rhombicity parameter E of Eu@C_{74} demonstrated the reduction of the symmetry from D_{3h} to C_{2v} due to the positioning of Eu^{2+} ion at the off-center of C_{74} cage. Moreover, in this work, the semiphenomenological superposition-exchange model (SPEM) was invoked to examine a relationship between the molecular structures and ZFS parameters. All of the experimental ZFS parameters were satisfactory reproduced in terms of the SPEM, leading to confirmation of the molecular symmetries. The semiphenomenological analysis also enabled us to select the most appropriate cage for Eu@C_{82} with C_2 symmetry from among three possible isomers.

Introduction

The structural determination of metallofullerenes has been a central topic in the field of fullerene science in order to develop new routes to bulk production.[1] The author's group has isolated various types of metallofullerenes: three structural isomers of Tm@C_{82},[2] four isomers of Ca@C_{82},[3] one isomer of Ca@C_{74},[4] and others. Kuran et al. also reported the isolation of Eu@C_{74}.[5] There exist nine possible structures for the C_{82} cage according to the so-called isolated pentagon rule (IPR).[6] The molecular symmetries of the isolated metallofullerenes, M@C_{82} (M = the metal ions), have been determined directly by ^{13}C NMR spectroscopy: C_s, C_2, and C_{2v} for the three isomers of Tm@C_{82};[2] C_s, C_{3v}, C_2, and C_{2v} for the four isomers of Ca@C_{82}.[3] Furthermore, it was shown by ^{13}C NMR spectroscopy that the cage of Ca@C_{74} has D_{3h} symmetry as is predicted by the IPR.[4] Electron paramagnetic resonance (EPR) spectroscopy has also been a powerful tool to elucidate electronic and molecular structures of metallofullerenes.[1,7−12] For example, it was demonstrated by EPR spectroscopy that Gd@C_{82}−I has an $S = 3$ ground state due to the intramolecular antiferromagnetic coupling between $S = {}^1/_2$ spin on the cage and $S = {}^7/_2$ spin of the encapsulated Gd^{3+} ion.[10]

In this work, multifrequency EPR measurements were carried out for a family of europium metallofullerenes (Eu@C_n) to examine the cage structures. The Eu^{2+} ion has a half-filled 4f orbital, resulting in an $^8S_{7/2}$ ground state with vanishing orbital angular momentum. According to many workers, the ZFS is closely related to the crystal field surrounding the Eu^{2+} ion.[14−21] In this work, a reliable spectral analysis was achieved using a spin Hamiltonian considering the ZFS terms up to fourth order.[21] Including the fourth-order terms into the Hamiltonian is essential to determine precisely the value of the second-rank components. The semiphenomenological superposition-exchange model (SPEM) was also invoked to examine a relationship between the cage structures and second-rank ZFS components.[18] In this work, the examination of the second-rank ZFS components was performed for each isomer of Eu@C_{74} and Eu@C_{82} by the SPEM, and the most appropriate cage structure was selected from among three possible cages with C_2 symmetry. Our attention has also been paid to the molecular structure of Eu@C_{74}. Molecular orbital calculations of Ca@C_{74} predicted that the encapsulated Ca atom is located at an off-center position along a C_2 axis in the cage.[22,23] The prediction could not be directly confirmed by ^{13}C NMR spectroscopy due to the site-hopping motion of a Ca atom inside the cage.[4] On the other

* Corresponding author. Telephone: +81-49-271-7295. Fax: +81-49-271-7985. E-mail: rik@josai.ac.jp.
† Institute for Molecular Science.
‡ Tokyo Metropolitan University.
§ Osaka City University.
⊥ Josai University.

10.1021/jp031350l CCC: $27.50
Published on Web 08/20/2004

hand, as shown in this paper, EPR spectroscopy demonstrated that the prediction is true for Eu@C_{74}.

Experimental Section

Materials. Soot containing Eu@C_{82} was produced by direct current (400 A) arc discharge of Eu/C composite rods under a 300 Torr of He atmosphere. The atomic ratio of Eu/C was 0.8 %. Both the empty fullerenes and the metallofullerenes were extracted from the soot by refluxing with 1,2,4-trichlorobenzene for 8 h. The isolation of three isomers of Eu@C_{82} was accomplished by five-stage high performance liquid chromatography method, which is allmost the same procedure applied to Tm@C_{82}.[2] A purity of more than 99% of the sample was confirmed by laser time-of-flight mass spectrometry. In this paper, the three isomers are termed Eu@C_{82}(I), Eu@C_{82}(II), and Eu@C_{82}(III). The extraction and isolation of Eu@C_{74} were achieved in a manner similar to Kuran's one.[5]

EPR Measurements. Perpendicular-mode X-band CW-EPR measurements, in which an oscillating magnetic field ($\mathbf{B}_1$) is applied perpendicular to the static magnetic field ($\mathbf{B}_0$), were carried out with a Bruker E500 spectrometer. Parallel-mode X-band CW-EPR measurements ($\mathbf{B}_1//\mathbf{B}_0$) were carried out using a Bruker ESP300 spectrometer with a Bruker ER4116DM dual mode cavity. Cryogenic temperatures were obtained with an Oxford 910 helium gas-flow-temperature controller. Perpendicular-mode W-band EPR measurements were carried out by a Bruker E680 spectrometer. Temperature was controlled by an Oxford CF935 helium gas-flow cryostat.

EPR Spectral Analysis. Fine-structure EPR spectrum observed for Eu^{2+} ion with an $^8S_{7/2}$ ground state can be interpreted by the following spin Hamiltonian:

$$\hat{H} = \beta_e S \cdot g \cdot B + \sum_{k,q} f_k b_k^q O_k^q \quad \left(k \geq |q|,\ k = 2,4,\ f_2 = \frac{1}{3},\ \text{and}\ f_4 = \frac{1}{60}\right) \quad (1)$$

where the first term stands for the electron Zeeman interaction, and the remaining terms for the zero-field splittings (ZFS). O_k^q and b_k^q represent the Stevens operator and the ZFS parameter, respectively. Because the sixth-order terms are sufficiently small, they were neglected in the following spectral simulation. The ZFS parameter b_2^0 corresponds to the conventional parameter D, and $^1/_3 b_2^2$ corresponds to E. Inclusion of the fourth-order terms is crucial for precise determination of the D and E values.[21]

Computer simulation of EPR spectra was carried out by homemade software based on a hybrid-eigenfield approach, which we have proposed as a practical method for EPR spectral simulation.[20,21,24] In the simulation, resonance fields are calculated directly without any iteration procedure, based on the eigenfield method originally developed by Belford et al.[25] Transition probabilities are calculated by diagonalizing the eigen-energy matrix with the obtained resonance fields.[20,21,24] The hybridization enables us to calculate both resonance fields and transition probabilities not only in reasonable computational time but also with proper accuracy. It also facilitates the consideration of the Boltzmann distribution in the simulation. For $S \geq 1$ spin systems, local strains around the spin site causes the distribution of D and E values, leading to a broadening of the spectral line width. In this work, such a broadening effect was involved in the simulation by employing a statistical $D-E$ strain model proposed by Wenzel and Kim.[26]

Results and Discussion

Absorption Spectra Observed for Eu@C_{82} and Eu@C_{74}. In previous works,[2,29] it has been proved that metallofullerenes exhibit an identical spectral pattern in their UV−vis−near-IR absorption spectra when they have the same cage structure and charge state. The symmetry of the cage for Ca@C_{82} isomer has been assigned by a ^{13}C NMR measurement.[3] C_s, C_{3v}, C_2, and C_{2v} symmetries have been identified for four isomers of Ca@C_{82}, which were termed Ca@C_{82}(I), Ca@C_{82}(II), Ca@C_{82}(III), and Ca@C_{82}(IV), respectively. Eu@C_{82}(I), Eu@C_{82}(II), and Eu@C_{82}(III) exhibited absorption spectra identical with those of Ca@C_{82}(I), Ca@C_{82}(III), and Ca@C_{82}(IV), respectively, as shown in Figure 1, parts a−c. Therefore, molecular symmetries of Eu@C_{82}(I), Eu@C_{82}(II), and Eu@C_{82}(III) can be assigned to C_s, C_2, and C_{2v}, respectively. In addition, it is indicated that the Eu atom takes a divalent state in the C_{82} cage as well as in the C_{60} cage.[13] The molecular structure of Ca@C_{74} has also been assigned to D_{3h} by a ^{13}C NMR measurement.[4] As shown in Figure 1d, the agreement of the absorption spectrum of Eu@C_{74} with that of Ca@C_{74} indicated that the Eu atom takes a divalent state again, and that the cage structure of Eu@C_{74} has D_{3h} symmetry.

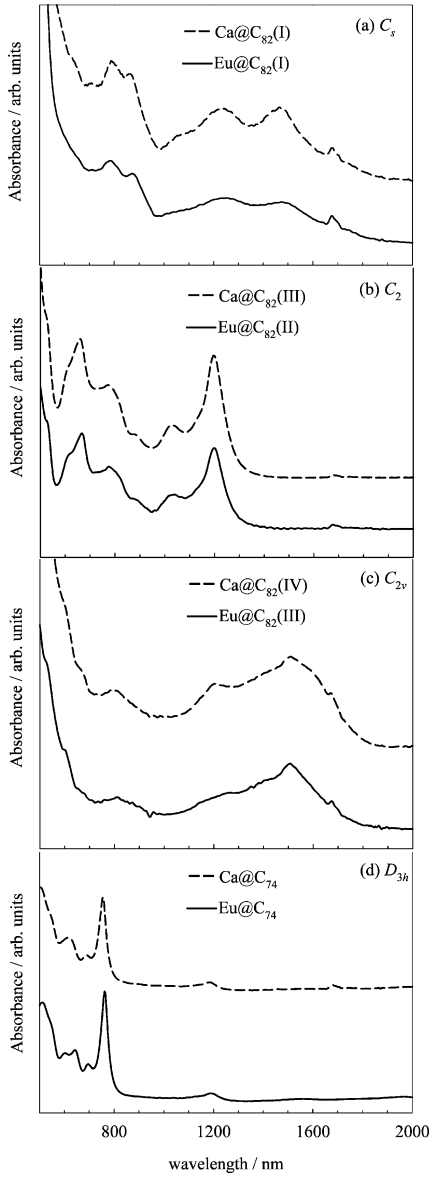

Figure 1. UV−vis−near IR absorption spectra of Ca@C_n and Eu@C_n in CS_2 solvent at room temperature: (a) Ca@C_{82}(I) and Eu@C_n(I) with C_s molecular symmetry, (b) Ca@C_{82}(III) and Eu@C_{82}(II) with C_2 molecular symmetry, (c) Ca@C_{82}(IV) and Eu@C_{82}(III) with C_{2v} molecular symmetry, and (d) Ca@C_{74} and Eu@C_{74} with the cage structure of D_{3h} symmetry.

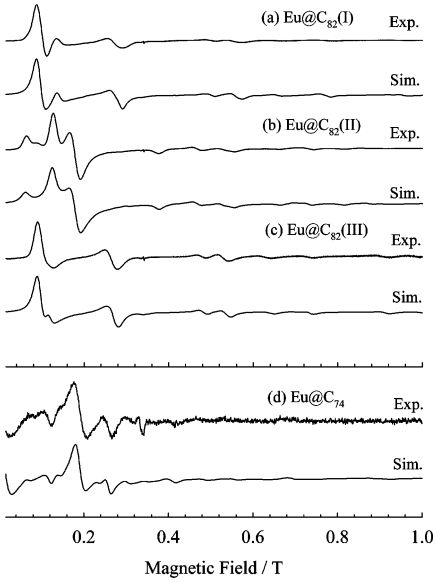

Figure 2. Perpendicular-mode X-band EPR spectra of Eu@C_n in CS_2 solvent: (a) Eu@C_{82}(I), (b) Eu@C_{82}(II), (c) Eu@C_{82}(III), and (d) Eu@C_{74}. Experimental conditions and simulation parameters: microwave frequency, 9.6 GHz; temperature, 1.5 K; line width, 24 mT.

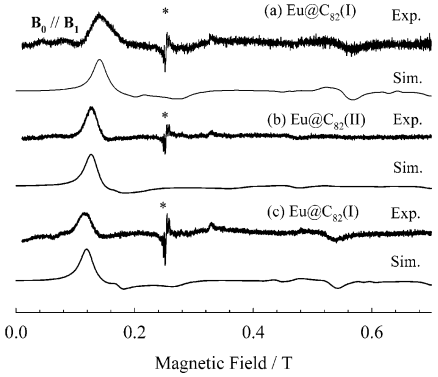

Figure 3. Parallel-mode X-band EPR spectrum of Eu@C_{82}: (a) Eu@C_{82}(I), (b) Eu@C_{82}(II), and (c) Eu@C_{82}(III) in CS_2 solvent. Experimental conditions and simulation parameters: microwave frequency, 9.4 GHz; temperature, 5 K; line width, 24 mT. Asterisks stand for a background signal from the cavity.

EPR Spectra Observed for Eu@C_n (n = 74 and 82). Parts a−d of Figure 2 show the perpendicular-model X-band CW-EPR spectra observed for Eu@C_{82}(I), Eu@C_{82}(II), Eu@C_{82}(III), and Eu@C_{74}, respectively. The observed asymmetric spectral features excluded the possibility that the magnitude of the ZFS is rather smaller than the X-band microwave energy ($\nu \sim 0.3$ cm^{-1}). In this work, parallel-mode X-band CW-EPR measurements were also carried out in order to confirm the determination of the values of the ZFS parameters. Parts a−c of Figure 3 show parallel-model X-band CW-EPR spectra observed for Eu@C_{82}(I), Eu@C_{82}(II), and Eu@C_{82}(III), respectively. The observation of an intense signal revealed that Eu@C_{82} has the same order of the ZFS as the X-band microwave energy. We also carried out W-band measurements in order to perform the straightforward determination of the spin-Hamiltonian parameters.[21] Parts a−d of Figure 4 show the observed W-band CW-EPR spectra of Eu@C_{82}(I), Eu@C_{82}(II), Eu@C_{82}(III), and Eu@C_{74}, respectively. They exhibit a symmetric pattern that can be easily assigned, illustrating that the electron Zeeman term dominates the ZFS in the W-band EPR measurement ($\nu \sim 3$ cm^{-1}). Moreover, in this work, temperature dependences of the W-band spectra were monitored in order to determine the signs of the b_2^0 values. As a typical example, the

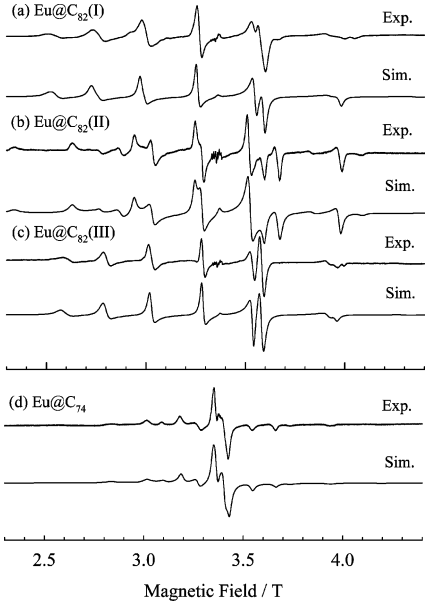

Figure 4. Perpendicular-mode W-band EPR spectra of Eu@C_n: (a) Eu@C_{82}(I), (b) Eu@C_{82}(II), (c) Eu@C_{82}(III), and (d) Eu@C_{74} in CS_2 solvent. Experimental conditions and simulation parameters: microwave frequency, 95 GHz; temperature, 20 K; line width, 24 mT.

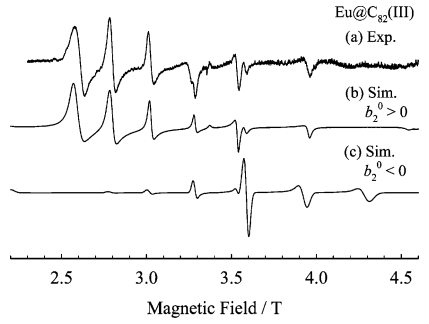

Figure 5. Perpendicular-mode W-band EPR spectrum of Eu@C_{82}(III) in CS_2 solvent: (a) experiment, and (b) simulations. The upper and lower simulations were calculated by using the positive and negative b_2^0 values, respectively. Experimental conditions and simulation parameters: microwave frequency, 95 GHz; temperature, 4 K; line width, 24 mT.

W-band spectrum of Eu@C_{82}(III) observed at 4 K is shown in Figure 5a. As described below, the spectral features indicate that the sign is positive. All of the spectra are completely reproduced by computer simulation based on the hybrid-eigenfield approach.

Computer Simulation of X- and W-Band Spectra. A reliable spectral analysis was achieved by the combined use of a perturbation treatment of the spin Hamiltonian and a spectral simulation based on the hybrid-eigenfield approach.[21] The ZFS terms up to the fourth order were considered in the spectral analyses. Parts a−d of Figure 4 show the calculated W-band CW-EPR spectra of Eu@C_{82}(I), Eu@C_{82}(II), Eu@C_{82}(III), and Eu@C_{74}, respectively. The spectral simulations were in good agreement with the observed spectra. The parameters obtained by the W-band simulation also gave well reproduced spectra for the perpendicular-mode X-band spectra, as shown in Figure 2. Moreover, the reliability of the parameters for Eu@C_{82}(I), Eu@C_{82}(II), and Eu@C_{82}(III) was confirmed by the simulation of the parallel-mode X-band spectra, as shown in Figure 3, parts a−c, respectively. The well-reproduced spectra proved that the encapsulated Eu atom takes the divalent state in the cages. The parameters precisely determined in this manner are given in Table 1. The fourth-rank ZFS components are considerably

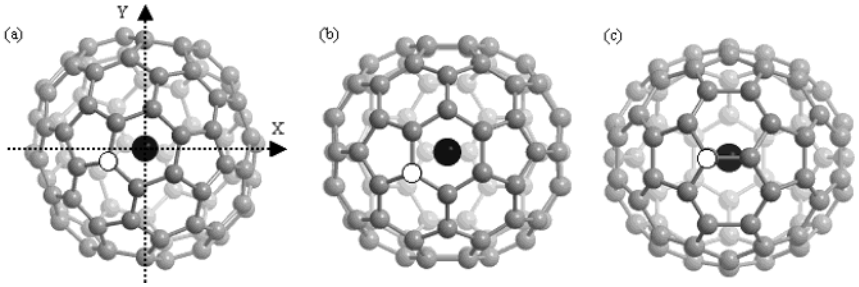

Figure 6. Molecular structures of (a) Eu@C_{82}(II), (b) Eu@C_{82}(III), and (c) Eu@C_{74}. The cage structure of part a corresponds to the C_2-c cage defined in Reference 30. Black and open circles stand for the Eu^{2+} ion and for the nearest carbon atom to the central ion, respectively. As shown in part a, the principal-axis orientations of the second-rank ZFS tensor are defined for all the metallofullerenes in terms of the SPEM. The *Z* principal axis is parallel to the C_2 symmetry axis, which is vertical to the paper.

TABLE 1: Spin-Hamiltonian Parameters Determined for the Europium Metallofullerenes

	Eu@C_{82}(I)	Eu@C_{82}(II)	Eu@C_{82}(III)	Eu@C_{74}
g_x	1.995	1.9919	1.9925	1.9938
g_y	1.993	1.9928	1.9921	1.9891
g_z	1.9946	1.9933	1.9939	1.9883
b_2^0/cm^{-1}	0.2918	0.2915	0.2724	0.1279
b_2^0/cm^{-1}	0.0074	0.0605	0.0041	0.00422
b_4^0/cm^{-1}	0.0008	0.0017	−0.0001	−0.0006
b_4^2/cm^{-1}	0.0033	−0.0032	−0.0003	0.0025
b_4^4/cm^{-1}	−0.0043	−0.0007	0.0021	−0.0023
mol. symmetry	C_s	C_2	C_{2v}	C_{2v} (D_{3h})

small compared with those of Eu-based luminescent materials.[21] As shown below, the difference can be interpreted by considering their molecular structures. In addition, it should be noticed that a nonzero rhombicity parameter E/D (=0.11) was obtained for Eu@C_{74}. The nonvanishing rhombicity parameter directly proves the deformation of the symmetry from D_{3h} to C_{2v} due to the positioning of Eu^{2+} ion off-center in the C_{74} cage.

The signs of the b_2^0 (=D) values were determined by analyzing the temperature dependences of the W-band spectra. As an example, Figure 5, parts b and c, shows W-band spectra of Eu@C_{82}(III) at 4 K calculated by using negative and positive b_2^0 values, respectively. Compared with the experimental spectrum in Figure 5a, it is obvious that Eu@C_{82}(III) has the positive b_2^0 value. The signs were also determined for the other samples in this manner, indicating that they are all positive.

Determination of Molecular Structures of the Metallofullerenes in Terms of the ZFS Parameters. The Eu^{2+} ion has a half-filled 4f orbital, resulting in an $^8S_{7/2}$ ground state with vanishing orbital angular momentum. Therefore, there exist no anisotropic terms in effective Hamiltonian within the framework of the second-order perturbation treatment of the spin−orbit interaction.[14−19] In fact, however, nonvanishing ZFS is observed in lower symmetry fields than cubic.[21] The superposition-exchange model (SPEM) can give a straightforward explanation of the ZFS of the Eu^{2+} ion.[18]

The essential assumption made in the SPEM is that the ZFS is produced by sums of individual contributions from neighboring ligands.[18] In the context of the SPEM, theoretical second-rank ZFS components are given as

$$b_2^q = \sum_i \bar{b}_2(R_i) G_2^q(\theta_i, \phi_i) \quad (q = 0, \pm 1, \pm 2) \tag{2}$$

where b_2^q stands for the second-rank ZFS components, and the summation is taken over all ligands. Also, $G_2^q(\theta_i, \phi_i)$ stands for the so-called "coordination factor", which depends on the angular positions (θ_i, ϕ_i) of ligands.[17c,d] R_i is the distance between the *i*-th ligand and the metal ion. The intrinsic parameter $\bar{b}_2(R_i)$ is defined as

$$\bar{b}_2(R_i) = \bar{b}_{EST}(R_0)\left(\frac{R_0}{R_i}\right)^3 + \bar{b}_{EXC}(R_0)\left(\frac{R_0}{R_i}\right)^{10} \tag{3}$$

where $\bar{b}_{EST}(R_0)$ and $\bar{b}_{EXC}(R_0)$ represent contributions from the electrostatic field of the ligand point charge and from the short-range metal−ligand interaction, respectively. In the SPEM analysis, $\bar{b}_{EST}(R_0)$, $\bar{b}_{EXC}(R_0)$, and the distance R_i are adjusted to reproduce the experimental ZFS components. According to Levin et al.,[18] R_0 is approximately equal to the distance equal to the sum of the ionic radii of the metal ion and the specific ligand, we fixed R_0 to be 2.8 Å in this work. Considering the molecular symmetry, we restrict the position of the Eu^{2+} ion for Eu@C_{82}(I) to the reflection plane, and those in Eu@C_{82}-(II), Eu@C_{82}(III), and Eu@C_{74} to the C_2 symmetry axis.

To determine the parameters $\bar{b}_{EST}(R_0)$ and $\bar{b}_{EXC}(R_0)$ for the Eu@C_n system, first we apply the SPEM to Eu@C_{82}(III) and Eu@C_{74}. Their cage structure is uniquely given as C_{2v} and D_{3h} (the total symmetry of C_{2v} in the case that the metal is positioned at off center) in terms of the IPR rule. The principal-axis orientations of the ZFS tensors are illustrated in Figure 6, parts b and c. The common value of 0.04 cm^{-1} for the parameter $\bar{b}_{EXC}(R_0)$ has been used independently of ligand types.[18] So we initially fixed the value of the parameter $\bar{b}_{EXC}(R_0)$ to be 0.04 cm^{-1}. Moving the metal position along the C_2 axis in the cage, we calculated the ZFS value according to eq 3 with various parameters $\bar{b}_{EST}(R_0)$. The deviations between calculated and experimental values were plotted as the function of the parameter $\bar{b}_{EST}(R_0)$ at each metal position. In the case of Eu@C_{82}(III) the deviation became zero solely when $\bar{b}_{EST}(R_0) = -0.220$ cm^{-1} with a nearest neighbor distance of 2.61 Å between the metal ion and the ligand. In the case of Eu@C_{74}, it became zero only at −0.270 cm^{-1} with 3.08 Å. The SPEM successfully predicted the experimental value of ZFS with a unique value of the parameter $\bar{b}_{EST}(R_0)$ at the specific metal position in each system. As a result, it can be concluded that the parameters $\bar{b}_{EXC}(R_0)$ and $\bar{b}_{EST}(R_0)$ used here are appropriate for the systems of Eu@C_{82} and Eu@C_{74}, and that the experimental values of ZFS are satisfactory reproduced by the metal position with the nearest neighbor distances at 2.61 and 3.08 Å, respectively. The metal position obtained here was quite coincident with that predicted by the *ab initio* calculations of Ca@C_{82}.[27] It should be noted that the absolute value of $\bar{b}_{EST}(R_0)$ for the bigger fullerene cage of Eu@C_{82} is smaller than that for Eu@C_{74}, considering that this parameter represents contributions from the electrostatic field of the ligand point charge.

By using the parameters $\bar{b}_{EXC}(R_0) = 0.04$ cm^{-1} and $\bar{b}_{EST}(R_0) = -0.220$ cm^{-1} obtained above for Eu@C_{82}, the ZFS components of Eu@C_{82}(II) were calculated by adjusting the metal position along the C_2 axis. The IPR rule gives three candidates

having different structures within the C_2 symmetry.[6,27] However, the SPEM can determine the unique cage structure which well reproduces the experimental ZFS with the principal-axis orientations shown in Figure 6a. The selected cage structure has the nearest neighbor distance between the metal ion and the ligand of 2.66 Å. It should be noted that not only the selected structure but also the predicted nearest neighbor distance is consistent with the prediction by ab initio calculations of $Ca@C_{82}$.[27]

Finally, the SPEM was applied to $Eu@C_{82}$(I) having three candidates for the cage structure predicted by the IPR.[6,27] The experimental ZFS components were actually reproduced by SPEM at some metal position in each cage. However, it was impossible to reduce three candidates to one because the metal's position within the cage could be found anywhere in the reflection plane of the Cs symmetry group.

Relationship between the Molecular Structures and Fourth-Rank ZFS Components. Theoretical treatment of the forth-rank ZFS component has not yet been completely achieved. Therefore, we discuss phenomenologically a relationship between the molecular structure and the fourth-rank ZFS component. Abraham et al. determined the fourth-rank components of Gd^{3+} and Eu^{2+} ions doped in various cubic fields composed of oxygen atoms, demonstrating that the absolute values of the components decrease sharply with increasing the metal−ligand distance.[28] For example, in the case of the Gd^{3+} ion, the absolute values are proportional to $R^{-9.5}$, where R stands for the metal−ligand distance. We have reported considerable fourth-rank ZFS components of the Eu^{2+} ion doped in strontium aluminates before.[21] Comparing with the Eu^{2+} ion doped in strontium aluminates, the absolute values of the forth-rank ZFS component are much smaller for Eu^{2+} ion encapsulated in $Eu@C_n$. Considering the longer metal−ligand distance of the metallofullerene with that of the Eu^{2+}-doped strontium aluminates, this result is reasonable.

Conclusions

This article demonstrated that the molecular symmetries of the $Eu@C_{82}$ were assigned to be C_s, C_2, and C_{2v} by comparing their absorption spectra with $Ca@C_{82}$. Multifrequency EPR measurements achieved the precise determination of the ZFS parameters including up to fourth order. It was for the first time experimentally proved that the Eu^{2+} ion in the $Eu@C_{74}$ is positioned at the off-center of the D_{3h} symmetry cage. All of the experimental ZFS parameters were well reproduced by the SPEM. As a result, it was concluded that the most stable cage of $Eu@C_{82}$(II) is C_2-c in the frame of the model. The SPEM analysis gave a reliable connection between the molecular structure and the ZFS parameters of the second-rank component as well as the fourth-rank one.

Acknowledgment. We thank Dr. K. Kobayashi (IMS) for providing the optimized geometries of the C_{82}^{2-} and C_{74}^{2-} cages. This work has been partly supported by Grants-in-Aid for JSPS Fellows from the Ministry of Education, Culture, Sports, Science, and Technology, Japan. H.M. acknowledges Research Fellowships of the Japan Society for the Promotion of Science for Young Scientists.

References and Notes

(1) For recent reviews, see the following: (a) Akasaka, T.; Nagase, S., Eds. *Endofullerenes: A New Family of Carbon Clusters*; Kluwer: Dordrecht, The Netherlands, 2002. (b) Shinohara, H. *Rep. Prog. Phys.* **2000**, *63*, 843.

(2) Kodama, T.; Ozawa, N.; Miyake, Y.; Sakaguchi, K.; Nishikawa, H.; Ikemoto, I.; Kikuchi, K.; Achiba, Y. *J. Am. Chem. Soc.* **2002**, *124*, 1452.

(3) Kodama, T.; Fujii, R.; Miyake, Y.; Sakaguchi, K.; Nishikawa, H.; Ikemoto, I.; Kikuchi, K.; Achiba, Y. *Chem. Phys. Lett.* **2003**, *377*, 197.

(4) Kodama, T.; Fujii, R.; Miyake, Y.; Suzuki, S.; Nishikawa, H.; Ikemoto, I.; Kikuchi, K.; Achiba, Y. In *Fullerenes and Nanotubes: The Building Blocks of Next Generation Nanodevices*; Kamat, P. V., Guldi, D. M., D'Souza, F., Eds.; The Electrochemical Society: Pennington, England, 2003; Vol. 13, p 548.

(5) Kuran, P.; Krause, M.; Bartl, A.; Dunsch, L. *Chem. Phys. Lett.* **1998**, *292*, 580.

(6) Fowler, P. W.; Manolopoulos, D. E. In *Atlas of Fullerenes*, Oxford University Press: Oxford, England, 1995.

(7) (a) Johnson, R. D.; de Vries, M. S.; Salem, J. R.; Bethune, D. S.; Yannoni, C. S. *Nature (London)* **1992**, *355*, 239. (b) Bethune, D. S.; Johnson, R. D.; Salem, J. R.; de Vries, M. S.; Yannoni, C. S. *Nature (London)* **1993**, *366*, 123.

(8) Kato, T.; Suzuki, S.; Kikuchi, K.; Achiba, Y. *J. Phys. Chem.* **1993**, *97*, 13425.

(9) Kato, T.; Bandou, S.; Inakuma, M.; Shinohara, H. *J. Phys. Chem.* **1995**, *99*, 856.

(10) Furuwaka, K.; Okubo, S.; Kato, H.; Shinohara, H.; Kato, T. *J. Phys. Chem. A* **2003**, *107*, 10933.

(11) Okubo, S.; Kato, T. *Appl. Magn. Reson.* **2003**, *23*, 481.

(12) Rubsam, M.; Pluschau, M.; Schweitzer, P.; Dinse, K.-P.; Fuchs, D.; Rietschel, H. R.; Michel, H.; Benz, M.; Kappesc, M. M. *Chem. Phys. Lett.* **1995**, *240*, 615.

(13) Inoue, T.; Kubozono, Y.; Kashino, S.; Takabayashi, Y.; Fujitaka, K.; Hida, M.; Inoue, M.; Kanbara, T.; Emura, S.; Uruga, T. *Chem. Phys. Lett.* **2000**, *316*, 381.

(14) Hutchison, C. A.; Judd, B. R.; Pope, D. F. D. *Proc. Phys. Soc. B* **1957**, *70*, 514.

(15) Wybourne, B. G. *Phys. Rev.* **1966**, *148*, 317.

(16) Sharma, R. R. In *Advances in Mossbauer spectroscopy: applications to physics, chemistry, and biology*; Thosar, B. V., Iyengar, P. K., Srivastava, J. K., Bhargava, S. C., Eds.; Elsevier: New York, 1983; Chapter 13.

(17) (a) Newman, D. J. *Adv. Phys.* **1971**, *20*, 44−45. (b) Newman, D. J.; Urban, W. *Adv. Phys.* **1975**, *24*, 793. (c) Newman, D. J.; Ng, B. *Rep. Prog. Phys.* **1989**, *52*, 699. (d) Newman, D. J.; Ng, B., Eds. In *Crystal Field Handbook*; Cambridge University Press: Cambridge, England, 2000.

(18) (a) Levin, L. I.; Cherepanov, V. I. *Sov. Phys. Solid State* **1983**, *25*, 394. (b) Levin, L. I.; Cherepanov, V. I. *Sov. Phys. Solid State* **1983**, *25*, 399. (c) Levin, L. I. *Phys. Status Solidi b* **1986**, *134*, 275. (d) Levin, L. I.; Eriksonans, K. M. *J. Phys. C: Solid State Phys.* **1987**, *20*, 2081. (e) Levin, L. I.; Goflov, A. D. *J. Phys.: Condens. Matter* **1992**, *4*, 1981.

(19) Eremin, M. V.; Antonova, I. I. *J. Phys. Condens. Matter*, **1988**, *10*, 5567.

(20) (a) Sato, K.; Matsuoka, H.; Shiomi, D.; Takui, T.; Itoh, K. *Mol. Cryst. Liq. Cryst.* **1999**, *334*, 1045. (b) Matsuoka, H.; Sato, K.; Shiomi, D.; Takui, T. *Synth. Met.*, **2001**, *121*, 1822. (c) Matsuoka, H.; Sato, K.; Shiomi, D.; Takui, T. *Appl. Magn. Reson.* **2003**, *23*, 517.

(21) Matsuoka, H.; Furukawa, K.; Sato, K.; Shiomi, D.; Kojima, Y.; Hirotsu, K.; Furuno, N.; Kato, T.; Takui, T. *J. Phys. Chem. A* **2003**, *107*, 11539.

(22) Wan, T. S. M.; Zhang, H.-W.; Nakane, T.; Xu, Z.; Inakuma, M.; Kobayashi, K.; Nagase, S. *J, Am. Chem. Soc.* **1998**, *120*, 6806.

(23) Nagase, S.; Kobayashi, K.; Akasaka, T. *J. Mol. Struct.* (*THEOCHEM*) **1999**, *461*−*462*, 97.

(24) For recent reviews, see the following: (a) Takui, T.; Sato, K.; Shiomi, D.; Itoh, K. In *Magnetic Properties of Organic Materials*; Lahti, P. M., Ed.; Marcel Dekker: New York, 1999; Chapter 11. (b) Takui, T.; Itoh, K. In *Molecular Magnetism; New Magnetic Materials*; Itoh, K.; Kinoshita, M., Eds.; Kodansha and Gordon & Breach: Tokyo and Amsterdam, 2000; Chapter 3. (c) Takui, T.; Matsuoka, H.; Furukawa, K.; Nakazawa, S.; Sato, K.; Shiomi, D. In *EPR of Free Radicals in Solids; Trends in Methods and Applications*; Lund, A., Shiotani, M., Eds.; Kluwer Academic Publishers: Boston, MA, 2003; Chapter 11.

(25) Belford, G. G.; Belford, R. L.; Bukhalter, J. F. *J. Magn. Reson.* **1973**, *11*, 251.

(26) Wenzel, R. F.; Kim, Y. W. *Phys. Rev.* **1965**, *140*, A1592.

(27) (a) Kobayashi, K.; Nagase, S. *Chem. Phys. Lett.* **1997**, *274*, 226. (b) Nagase, S.; Kobayashi, K.; Akasaka, T. *J. Comput. Chem.* **1998**, *19*, 232.

(28) Abraham, M. M.; Boatner, L. A.; Chen, Y.; Kolopus, J. L.; Reynolds, R. W. *Phys. Rev. B* **1971**, *4*, 2853.

(29) Wakahara, T.; Okubo, S.; Kondo, M.; Maeda, Y.; Akasaka, T.; Waelchli, M.; Kako, M.; Kobayashi, K.; Nagase, S.; Kato, T.; Yamamoto, K.; Gao, X.; Van Caemelbeche, E.; Kadish, K. M. *Chem. Phys. Lett.* **2002**, *360*, 235.